Construction and Building Materials 313 (2021) 125494

Contents lists available at ScienceDirect

Construction and Building Materials

journal homepage: www.elsevier.com/locate/conbuildmat

The utilization of waste incineration filter dust (WIFD) in sodium carbonate activated slag mortars

Xuan Ling [a,b], Katrin Schollbach [b], Gang Liu [c,*], H.J.H. Brouwers [a,b]

[a] State Key Laboratory of Silicate Materials for Architectures, Wuhan University of Technology, Wuhan 430070, China
[b] Department of the Built Environment, Eindhoven University of Technology, 5612 AP Eindhoven, the Netherlands
[c] School of Human Settlements and Civil Engineering, Xi'an Jiaotong University, Xi'an 7100499, China

ARTICLE INFO

Keywords:
Waste incineration filter dust
GGBFS
Sodium carbonate
Microstructure
Alkali-activation

ABSTRACT

The presented work utilizes Waste Incineration Filter Dust (WIFD) as a green ingredient in a sodium carbonate activated ground granulated blast furnace slag (GGBFS) system. WIFD is produced with a high portlandite and calcite content in MSWI incineration plants. The reaction kinetics and reaction products of the system are analyzed through isothermal calorimetry, X-Ray diffraction (XRD), thermogravimetric analysis (TG-DTG), FT-IR, SEM/BSE/EDX, BET tests. The flowability and compressive strength of WIFD mixed samples are evaluated. The results show that the WIFD and Na_2CO_3 have a synergistic effect on the activation of GGBFS. The portlandite from WIFD could replace the pure $Ca(OH)_2$ and react with Na_2CO_3 to improve the alkalinity. The incorporation of WIFD accelerates the Na_2CO_3 activated GGBFS with the main products, including C-(A)-S-H gel, hydrotalcite and hemicarbonate. Besides, the calcite from WIFD is beneficial to form the hemicarbonate and decrease the porosity of the matrix. Though the mechanical performance of samples is reduced with more WIFD, it's still high enough for a potential application in construction with lower strength requirements. The results also confirm that GGBFS could be activated by WIFD along and the addition of sodium carbonate helps the strength development and increases reaction speed. The work shows the potential of WIFD applying as a green building material.

1. Introduction

To reduce the CO_2 emission and huge consumption of natural resources for production of normal cement based building materials, various by-products from industries have been investigated to partially replace normal cement during concrete casting [15,29,30,44–47,50]. However, the cement clinker is still necessary for the performance development of blended cement concrete. As a cement-free binder, alkali-activated materials (AAMs) have attracted great attention because of their low CO_2 emissions and comparable mechanical performance compared to ordinary Portland cement (OPC) [12,37,52]. Ground granulated blast furnace slag (GGBFS) is one of the most common materials for the design of alkali-activated systems [5,20,27,41,51,56]. It can be activated by hydroxides (MOH), carbonates (M_2CO_3) and silicates (M_2SiO_3) (M represents the alkali ion) [3,14,22,28,38]. The application of various activators in the reaction system shows significant effects on the reaction kinetics, the formation of reaction products and the physical performance of the binder. Generally, MOH and M_2SiO_3 contribute to a fast reaction of AAMs; consequently, better performance can be achieved. However, the intensive reaction results in fast degradation of workability and high shrinkage [26,57]. In addition, the production of hydroxides and silicates usually accounts for very high energy consumption. The high alkalinity of activators also can cause a safety risk during the construction process. To overcome these defects, the Na_2CO_3 activated materials with lower alkalinity were investigated, the reaction products are mainly hydrotalcite, gaylussite and C-(A)-S-H gel [53], which shows lower shrinkage as well as costs and safety risks compared to normal AAMs activated by hydroxides and water glass [10].

However, the activation of GGBFS by Na_2CO_3 is slow due to the lower initial pH compared to the NaOH. Several works verified the slow reaction process of Na_2CO_3 activated GGBFS and unsatisfied early strength development during the early reaction period [22,53]. Therefore, an accelerated setting time and improved early strength development are essential for Na_2CO_3 activated AAMs. Several approaches have been proposed to enhance the performance of Na_2CO_3 activated AAMs. For example, the additives such as $Mg(OH)_2$ and MgO play the role of filler to decrease the porosity of the binder [1,42]. Calcined layered

* Corresponding author.
E-mail address: gang.liu@xjtu.edu.cn (G. Liu).

https://doi.org/10.1016/j.conbuildmat.2021.125494
Received 21 August 2021; Received in revised form 8 October 2021; Accepted 29 October 2021
Available online 9 November 2021

double hydroxides [22], calcined dolomite [50], limestone powder [54] and $Ca(OH)_2$ [18,48] were reported in the Na_2CO_3 activated AAMs to accelerate the consumption of CO_3^{2-} ions and improve the initial pH value of the pore solution [19], consequently, the early age performance can be improved. Notably, the chemical method shows more effectiveness and efficiency in the early strength development of the binder. Compared to other calcined additives, $Ca(OH)_2$ and limestone draw more attention due to their low costs and wide distributions. However, the usage of high pure $Ca(OH)_2$ dosages in the alkali-activated materials may cause safety issues, while the production of $Ca(OH)_2$ releases large amounts of CO_2 into the atmosphere due to the calcination of raw materials [16]. Therefore, the demand for proposing the green and economic alternates as new additives in sodium carbonate activated materials to enhance early age reaction is required.

Waste incineration filter dust (WIFD) is a new stream of solid waste in the Netherlands, which is produced during the incineration process of municipal solid wastes by injection of a suspension of quick lime in the hot flue gas. As a kind of air pollution control residue (APC), WIFD is formed to remove sulfur dioxide from the emission gases in incineration plants in the Netherlands. Generally, these kinds of residues are only disposed of in landfilling or road base construction, which would be a waste of its highly reactive calcium content [36]. The potential treatment for APC residues can be as separation processes, solidification/stabilization and thermal methods [34]. However, these procedures take more time and extra cost. And while the WIFD is always rich in portlandite and calcite, its composition can vary widely, making the treatments more complicated. Shirley et. al also proposed to use a co-fired pulverized fuel ash to solidify the air pollution control residues [39]. Therefore, it is possible and convenient to apply WIFD in sodium carbonate activated materials as a green and low-cost additive. The calcium hydroxide and calcite may play the role of accelerator for enhancing the reaction process of sodium carbonate activated GGBFS based on the above research review. According to the present data, nearly 5 kt/yr of WIFD were produced per year for air pollution control in the incineration plant in the Netherlands. Because of the relatively low production of WIFD compared with the alkali-activated slag binders, all WIFD could be recycled while uses the optimal content of 5% wt. The reuse of the WIFD in the AAMs has advantages both in the cost and energy savings, CO_2 emission and waste management.

In this study, the early reaction of Na_2CO_3 and portlandite from WIFD was designed to improve the alkalinity of pore solution, which is beneficial for early strength development. The influences of Na_2CO_3 and WIFD on alkali-activated GGBFS were investigated. The couple effects of Na_2CO_3 and WIFD on the reaction products, reaction kinetics and mechanical properties of this cement-free binder were investigated. The X-ray diffraction (XRD), thermo-gravity (TG), Fourier transform infrared spectroscopy (FT-IR) and the Scanning Electron Microscope (SEM) with EDX analysis were conducted. The related results can provide a new application of WIFD in sodium carbonate activated materials.

2. Materials and methods

2.1. Characterization of materials

Ground granulated blast furnace slag (GGBFS) used in this study was provided by ENCI, IJmuiden, Netherlands. The waste incineration filter dust (WIFD) in Fig. 1 (a) was provided by Euro Trust Management, Netherlands. The chemical compositions of raw materials were measured using X-ray fluorescence (PANalytical Epsilon 3) and are shown in Table 1. Sulfur and calcium are the main elements in WIFD. The mineral compositions in Fig. 1 (b) show that the main crystalline phases of WIFD are calcite (PDF#47-1743), portlandite (PDF#44-1481) bassanite (PDF#24-1068) and dolomite (PDF#73-2409). The portlandite and calcite amounts are 36.38% and 37.43%, respectively, calculated from TG results in Fig. 2, which accounts for the high LOI of WIFD. The particle size distributions of GGBFS and WIFD are shown in

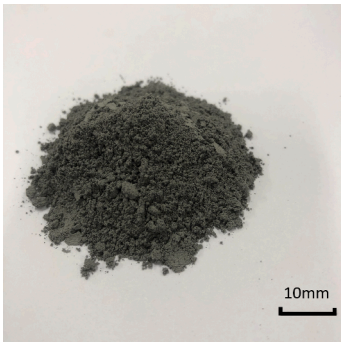

(a)

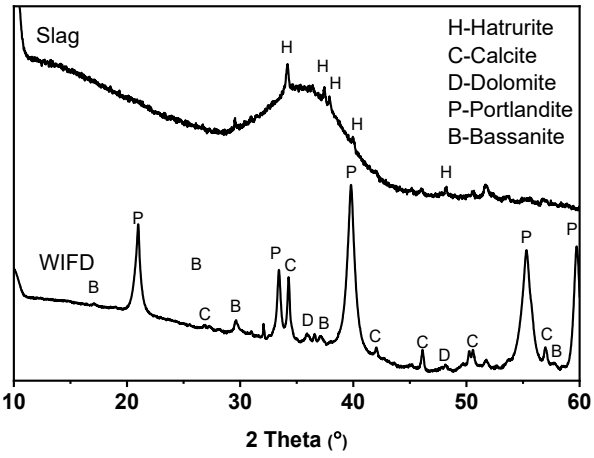

(b)

Fig. 1. Raw material and XRD pattern of Waste incineration filter dust (WIFD) and GGBFS.

Fig. 3. The average particle size of GGBFS and WIFD is around 13 μm. The chemical composition of the leachates obtained from WIFD via one batch leaching test is presented in Table 2. The high Ca^{2+} and SO_4^{2-} concentration is coherent with the XRF results. Na_2CO_3 (powder, analytical grade, supplied by Sigma-Aldrich) was used to prepare the activator.

2.2. Testing methods

2.2.1. Isothermal calorimeter

The reaction kinetics were determined by an isothermal calorimeter (TAM Air, Thermometric) at 20 °C. The raw material was first mixed in a bottle according to the paste mixture. Then the water was added, and the content was mixed with a vortex mixer. The mixed paste was injected into a sealed glass ampoule and loaded into the calorimeter for 6 days. The heat release and heat flow results were normalized by mass (g) of the binder.

2.2.2. Leaching test

To assess the leaching potential of the WIFD, a one-batch leaching test was employed according to NEN-EN12457-4. WIFD powder and distilled water were mixed in a polyethylene bottle with a solid to liquid mass ratio of 1/10. The bottle was placed horizontally on a liner reciprocating shaking device (Stuart SSL_2) at a rate of 250 rpm for 24 h. Then the leachate samples were filtered with a 0.2 um PTFE filter and acidified with ultrapure nitric acid. The leaching analysis was conducted with ion chromatography (IC) and inductively coupled plasma optical emission spectroscopy (ICP-OES).

Table 1
Chemical compositions of raw materials.

ChemicalComposition	Na_2O	MgO	Al_2O_3	SiO_2	SO_3	K_2O	CaO	TiO_2	Fe_2O_3	Cl	LOI%	Surface aream^2/g	Specific densityg/cm^3
WIFD	0.15	0.73	0.20	0.59	6.51	0.21	53.97	0.02	0.70	0.62	36.24	25.1	2.32
GGBFS	/	9.02	13.09	31.24	5.15	0.29	38.56	1.3	0.67	0.04	0.64	1.0	2.93

*LOI = loss on ignition at 1000C for 2 h.

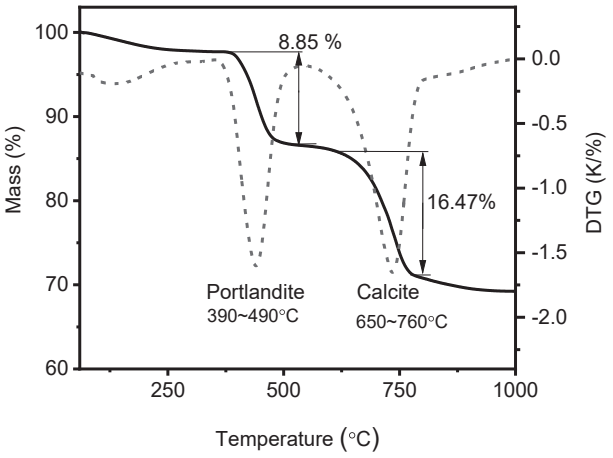

Fig. 2. TG and DTG curves of Waste incineration filter dust (WIFD).

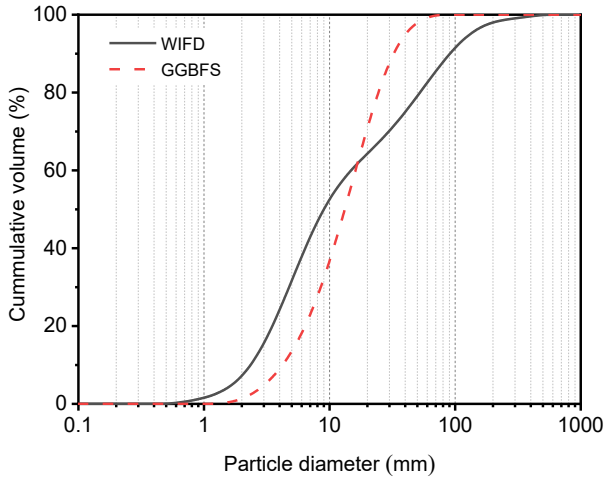

Fig. 3. Particle size distribution of each raw material.

2.2.3. Phase assemblage analysis

The phase composition of paste samples was characterized by X-ray diffraction (XRD), thermal gravity (TG) and Fourier transform infrared spectroscopy (FT-IR). The paste samples were broken into small pieces by an iron hammer and immersed into isopropanol to stop the hydration process for 24 h. Then the samples were dried at 60 °C for 24 h and grounded in an agate mortar until passing the 75 μm sieve for further analysis.

The dried powder samples were measured by a Bruker D4 phaser instrument with a step size of 0.02° and a 2θ range from 10° to 90° (Co-K_α, 40 kV, 30 mA).

The thermo-gravimetric (TG) test was conducted using a STA 449 F1 instrument under N_2 atmosphere at a heating rate of 10 K/min up to 1000 °C. Differential thermo-gravity (DTG) results are calculated from thermo-gravity (TG). The quantification of calcite and $Ca(OH)_2$ content was calculated by using the mass loss during different decomposition temperature ranges in TG, for example, 600℃ to 850 ℃ for calcite [35], and 390℃ to 500℃ for $Ca(OH)_2$ [23].

Fourier-transform infrared (FT-IR) spectroscopy was conducted by using Varian 3100 instrument to identify the bonding in the mineral phases and the amorphous contents in samples with the wavenumber range of 4000–400 cm^{-1}.

2.2.4. Fresh behavior and mechanical test of mortars

The flowability of the fresh mortars was determined using the mini spread flow table test according to EN 1015-3:2007.

The mechanical properties of the mortar are studied according to EN 196–1:2016. The samples covered by the plastic film with a size of 40 × 40 × 160 mm^3 curing at ambient temperature were tested at a loading rate of 2400 N/s for compressive strength after 7 days, 28 days and 91 days. Compressive strength tests were conducted on 6 specimens for each mixture.

2.2.5. Microstructure analysis of reaction products

The microstructure of paste samples after 28 days of curing was observed by using Scanning Electron Microscope with EDX (15KV) detector (Phenom Pro). The crushed samples were immersed in isopropanol to stop the reaction process and dried at 40 °C for 24 h. Afterward, the samples were embedded in resin and polished with grinding papers. The polished surface was then coated with Au by using Quorum 150TS plus sputter coater.

The Nitrogen sorption analysis of dried samples was conducted by using TriStar II 3020, Micrometrics. The powder samples (less than400 um) were dried at 105℃ until the mass was constant before the test. The gel pore size distribution was calculated from the adsorption branch by the Barrett - Joyner - Hallenda method [7].

2.3. Sample preparations

In this study, two sets of paste and mortar samples were prepared according to the mix proportions in Table 3. To study the influences of WIFD on the performance of sodium carbonate activated GGBFS, In the first set the amount of Na_2CO_3 was 8 % (equivalent sodium oxide (Na_2O) content of 4.6 wt% by weight of binder), while the amount of WIFD was from 0 %, 5 %, 10 %, 15 % to 20 %. To reveal the effects of Na_2CO_3 concentration on GGBFS-WIFD binder systems, the second set was prepared as follows, that the amount of WIFD was kept constant (10 %) and the amount of Na_2CO_3 was varied (2.3 %, 4.6 % and 6.9 % of total mass of WIFD and GGBFS). The water/binder ratio by mass was 0.5 for paste and 0.6 for the mortar to meet the water demand of the fine aggregates. The sand/binder ratio was 3.0 for mortar samples.

All the samples were mixed in a laboratory mixer. The binder and sand were well dispersed and then the water was added at a low speed

Table 2
Leaching behavior of WIFD obtained via a one-batch leaching test.

Parameters	K	Ca	Na	Mg	Al	Ba	Sr	Zn	Fe	NO_3^-	SO_4^{2-}	Cl^-	pH
WIFD[mg/kg]	1360	17,510	2280	0.21	0.01	3.5	70.29	1.14	0.01	310	13,430	5910	12.98

Table 3
Mix proportions of paste and mortar specimens.

Sample	Na_2CO_3/% (Na_2O%)	Waste/ g	Slag/ g	Sand/g	w/b
N8W0	8 (4.6)	0	100	0(paste)300 (mortar)	0.5(paste)0.6 (mortar)
N8W5	8(4.6)	5	95		
N8W10	8(4.6)	10	90		
N8W15	8(4.6)	15	85		
N8W20	8(4.6)	20	80		
N0W10	0(0)	10	90		
N4W10	4(2.3)	10	90		
N12W10	12(6.9)	10	90		

for 30 s. Then stop the mixer 30 s for stirring the bottom specimens. After another 120 s mixing at a medium speed, the samples were poured into $40 \times 40 \times 160\ mm^3$ styrofoam molds and vibrated for 1 min. After 1-day curing, the specimens were demolded and sealed with plastic films, then stored under laboratory conditions with 50% RH and 20 °C.

3. Test results and discussion

3.1. Flowability of NC-WIFD-GGBFS mortars

The flowability of the fresh mortars is shown in Fig. 4. The N8W0 shows a satisfied flowability of 250 mm. After the WIFD gradually replaced the GGBFS, the workability of mortar decreased significantly. The high surface area of WIFD compared to GGBFS induces a high water demand for blends. On the other hand, the increase of Na_2CO_3 in the activator also reduced the workability of mixtures containing 10% of WIFD. It can be seen in Fig. 5, sample without Na_2CO_3 shows a flowability of 180 mm, and it gradually decreased to 130 mm when Na_2CO_3 increased to 12%. The increased Na_2CO_3 dissolved in the solution would accelerate the calcium consumption in pore solution and promote the formation of carbonates. The increased precipitation of carbonates inhibits the flow of mortars. The above results indicate that the addition of Na_2CO_3 and WIFD reduces workability due to the fast precipitation reaction between Na_2CO_3 and the high surface area of WIFD.

3.2. Reaction kinetics of NC-WIFD-GGBFS blends

To study the effects of WIFD and Na_2CO_3 on the reaction process of various mixtures, the calorimeter test was conducted, and the results are shown in Fig. 6 (a). As can be seen, the increased WIFD in mixtures obviously accelerates the reaction process, reducing the duration of the induction period. In N8W0, two exotherm peaks occur at around 4 h and

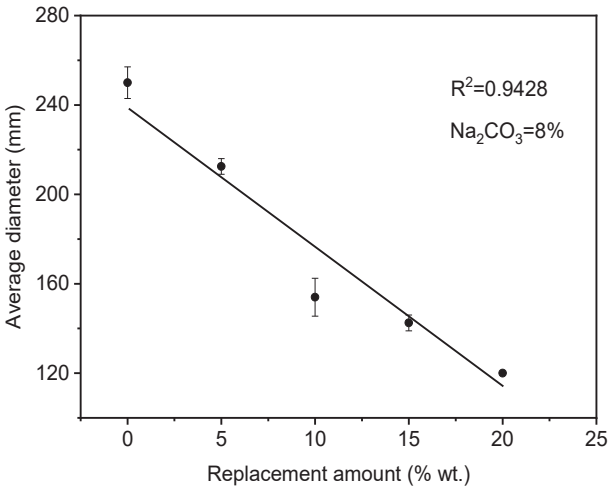

Fig. 4. Spread flow diameter of 8% Na_2CO_3 activated GGBFS mortars containing WIFD.

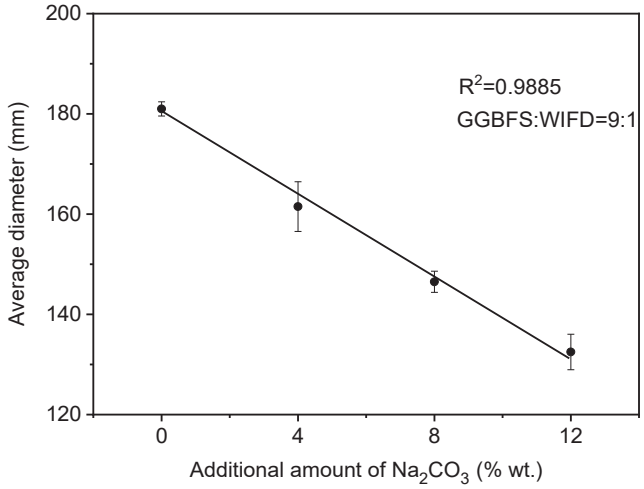

Fig. 5. Spread flow diameter of the GGBFS-WIFD mortars activated by different amounts of Na_2CO_3.

60 h after the initial peak caused by particle wetting and dissolution. The first small exotherm peak could be attributed to the formation of gaylussite ($Na_2Ca(CO_3)_2{\cdot}5H_2O$) and calcite, which are general reaction products in sodium carbonate activated GGBFS system [55]. The second main exotherm is assigned for the formation of C-(A)-S -H type gel as the main reaction products in sodium carbonate activated GGBFS system [55]. It takes nearly 2 days for sodium carbonate activated slag to reach the heat flow peak, which is consistent with some previous results that show even longer retardation when only Na_2CO_3 were used in the activator [4,11].

However, the heat flow curves become quite different and only one exotherm peak could be found after incorporating WIFD. The time to reach the main exotherm peaks was reduced to 9.79 h and 2.31 h when incorporating 5 % and 10 % WIFD, respectively. Then the reaction process shows no more significant improvement after the amount of WIFD is higher than 10%; for example, N8W15 takes 1.65 h and N8W20 takes 1.56 h to reach the main exotherm peak. The main reason is the amount of Ca^{2+} provided by the dissolving portlandite in WIFD is higher than the amount of Na_2CO_3 and the system becomes oversaturated. Nevertheless, the cumulative heat of each mixture increases with higher amounts of WIFD in the reaction as summarised in Table 4. Therefore, WIFD acts as an extra activator to accelerate the reaction process and shows the potential to be effectively applied in the Na_2CO_3 activated GGBFS.

The effect of Na_2CO_3 content on the reaction process of GGBFS-WIFD blends is shown in Fig. 7. N0W10 also shows a prolonged induction period, which is similar to the sample N8W0. It shows two exotherm stages at around 24 h and 51 h, respectively. The first exotherm as seen arrow can be induced by the formation of ettringite due to the existence of SO_3 and aluminate in raw materials. Then the main exotherm around 51 h is attributed to the formation of C-(A)-S-H gel and hemicarbonate as

Table 4
Summary of cumulative heat of samples at 144 h.

Group	Time (h)(to reach the heat flow peak)	Cumulative heat at144 h (J/g slag)
N8W0	58.06	190.40
N8W5	9.79	224.05
N8W10	2.31	225.96
N8W15	1.65	243.93
N8W20	1.56	209.55
N0W10	51.15	154.36
N4W10	3.53	149.16
N8W10	2.31	225.96
N12W10	2.38	244.89

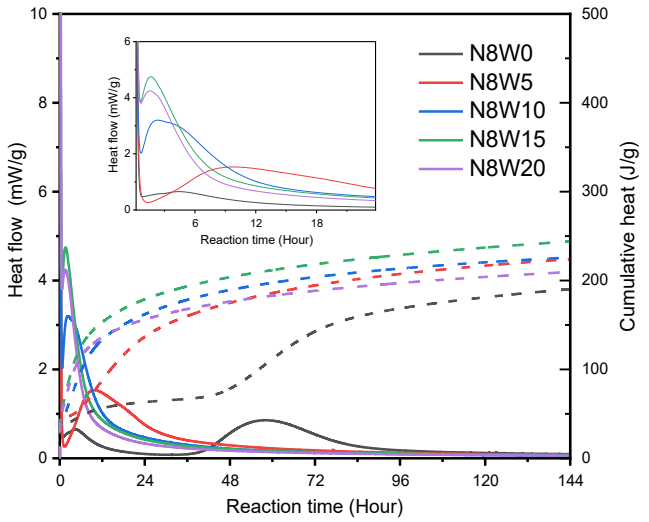

Fig. 6. Heat release of the Na_2CO_3 activated GGBFS with different WIFD replacements from 0% to 20% by mass.

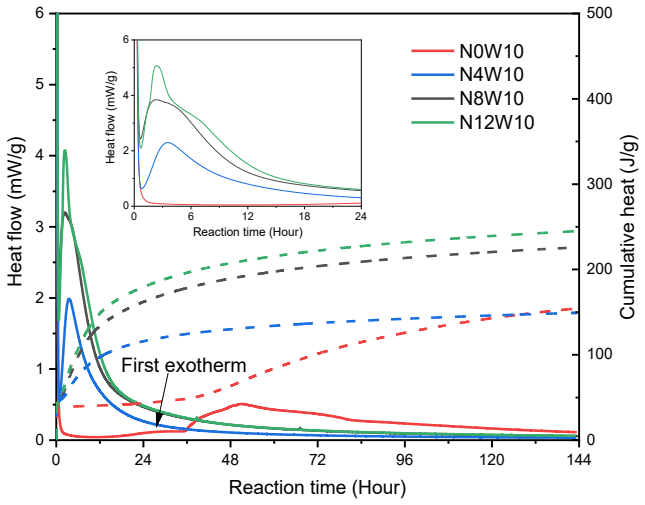

Fig. 7. Heat release of the 90% GGBFS and 10% WIFD blended binder with the additional amount of Na_2CO_3 from 0% to 12% by mass.

seen in Fig. 12. This indicates that only WIFD also can effectively activate GGBFS, which plays the role of activator. However, the pH it generates in N0W10 is lower because the OH^- provided by portlandite is limited, leading to a slower reaction process at early ages, which is consistent with the reported work about calcium hydroxide activated GGBFS [49].

In contrast to N0W10, incorporating Na_2CO_3 (N4W10, N8W10 and N12W10) results in only one exotherm followed by a small shoulder. The main peak is attributed to the formation of C-(A)-S-H gel and the small shoulder is probably a result of the other reaction products including hemicarbonate, hydrotalcite. Obviously, the additional Na_2CO_3 accelerated the reaction through the fast reaction with portlandite, and then the formation of sodium hydroxide; consequently, the reduction of time to reach the maximum hydration peak can be observed in Table 4. Meanwhile, the 144 h cumulative heat increases from 149.16 J/g in N4W10 to 244.89 J/g in N12W10. It could be explained that more GGFBS can be activated when higher Na_2CO_3 content is. However, the 144 h cumulative heat of N4W10 is lower than that of N0W10 (154.36 J/g) which could be explained by additional heat generated by the ettringite formation. The additional Na_2CO_3 in N4W10 probably induces the formation of calcium carbonates rather than the ettringite. To conclude, a synergistic effect between Na_2CO_3 and WIFD can be spotted during the activation of GGBFS. The presence of WIFD effectively overcomes the retardation effects of Na_2CO_3 activated GGBFS.

3.3. Reaction products identification of NC-WIFD-GBS blends

3.3.1. XRD analysis

The X-ray diffraction patterns of Na_2CO_3 activated GGBFS samples with different WIFD replacement ratios after 28 days of curing are shown in Fig. 8. The main crystalline phases in samples are hydrotalcite ($Mg_6Al_2CO_3(OH)_{16}{\cdot}4H_2O$) (PDF#89–0460), calcite (PDF#72–1937), dolomite (PDF#75–1759), hemicarbonate ($3CaO{\bullet}Al_2O_3{\bullet}0.5Ca(OH)_2{\bullet}0.5CaCO_3{\cdot}11.5H_2O$) (PDF# 41–0221) and dolomite (PDF#75–1759), along with the portlandite ($Ca(OH)_2$) and calcite (PDF#72–1937) from the WIFD. Only the reference (N8W0) contains gaylussite ($Na_2Ca(CO_3)_2{\cdot}5H_2O$) (PDF#74–1235), which is not observed in samples N8W5-N8W20, indicating that the increased WIFD may inhibit the formation of gaylussite. After 28 days of curing, the increased intensity of hemicarbonate, hydrotalcite, calcite, dolomite in each sample indicates that the increasing WIFD content promotes the formation of carbonates in the reaction system. Notably, C-(A)-S-H gel, which is well known to be produced as the main reaction product in the alkali-activated GGBFS with low crystallinity, so it is hard to see in XRD patterns [24]. Additionally, the main specific peak overlaps with that of calcite around 34.2°(2θ).

Fig. 9 shows the reaction products formation of N8W10 at different ages. The main phase composition in N8W10 shows little difference after a 1-day reaction, as the main reaction has taken place after 24 h from the calorimetric test results shown in Fig. 6. The main reaction products are the same as mentioned above. However, the intensity of the specific peaks of hemicarbonate and hydrotalcite shows a variation at a late age.

The effects of Na_2CO_3 content on reaction products of mixtures containing 90% GGBFS and 10% WIFD after 28 days of curing are shown in Fig. 10. The main reaction products are calcite, dolomite, ettringite, hydrotalcite and hemicarbonate in the sample of blended GGBFS and WIFD without Na_2CO_3 (N0W10), which confirms the activation effect of WIFD on the GGBFS. After the Na_2CO_3 was applied in the activator, the peaks of ettringite were not observed in mixtures (N4W10-N12W10).

Fig. 11 shows the XRD patterns of sample N0W10 at different curing ages. The peaks of ettringite and calcite are identified after 1 day of reaction, which may contribute to the first exotherm in N0W10 at around 24 h in the calorimetric test results in Fig. 7. Then hemicarbonate and dolomite were observed in the sample after 3 days reaction in the XRD patterns, which may also contribute to the main

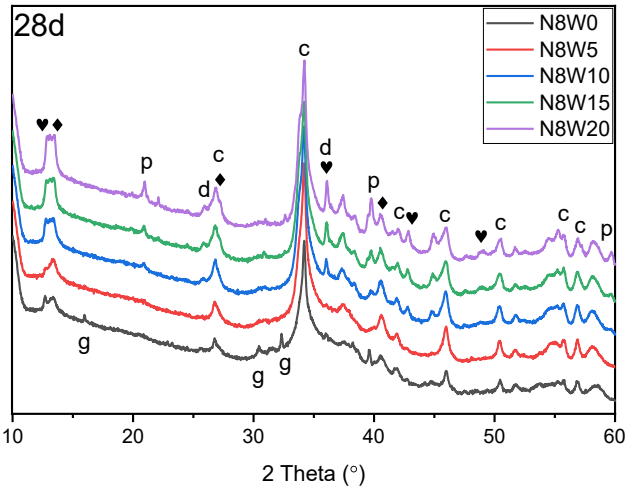

Fig. 8. XRD patterns of samples with different replacement of WIFD after 28 days curing (c-Calcite, d-Dolomite p-Portlandite, ♥- Hemicarbonate, ◆ - Hydrotalcite, g- Gaylussite).

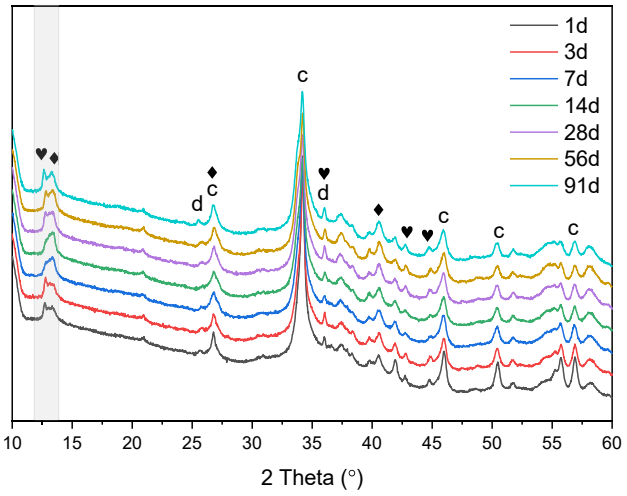

Fig. 9. XRD patterns of sample N8W10 at different curing ages (c-Calcite, d-Dolomite ♥- Hemicarbonate, ◆ - Hydrotalcite).

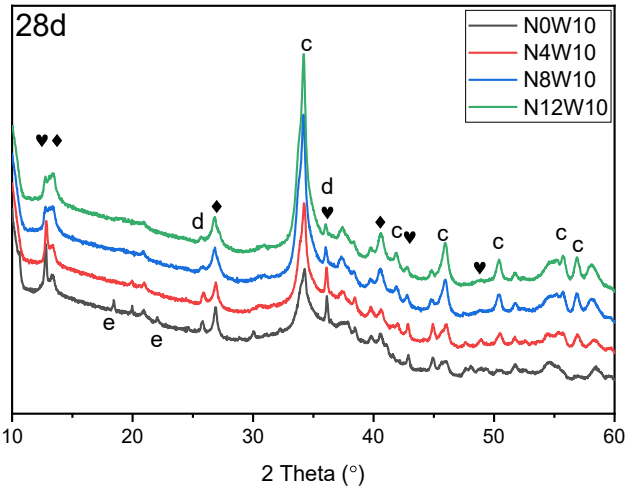

Fig. 10. XRD patterns of samples with additional Na_2CO_3 after 28 days curing (c-Calcite, d-Dolomite, ♥- Hemicarbonate, ◆ - Hydrotalcite, e-Ettringite).

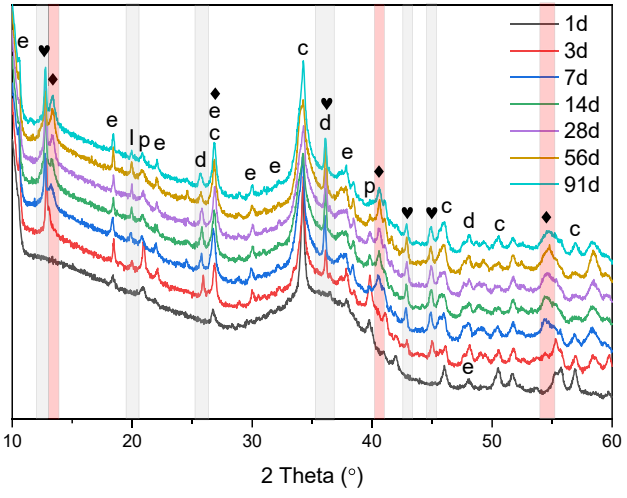

Fig. 11. XRD patterns of sample N0W10 at different curing ages (c-Calcite, d-Dolomite p-Portlandite, ♥- Hemicarbonate, ◆ - Hydrotalcite, e-Ettringite, I-Ikaite) (Peaks marked grey and red first appear after 3 days, 7 days respectively).

exotherm in N0W10 around 51 h in Fig. 7. Then the peaks intensity of hydrotalcite gradually increases from 7 days to 91 days, which confirms the ongoing reaction process. The peak of Ikaite (PDF#75–1733) is not particularly sure for its low intensity and the overlap with other minerals.

3.3.2. FT-IR analysis

The phase assemblage of reaction products after 28 days' curing was characterized by FT-IR and the results are shown in Fig. 12. The content of WIFD shows no significant influence on the FT-IR results of reaction products as shown in Fig. 12 (a). The broad bands centered around 3405 cm^{-1} and 1649 cm^{-1} present the stretching and bending mode of the H–OH bond in the samples. These resonances may be caused by the bound water or interlayer water from gaylussite or C-(A)-S-H gels [17]. The absorption peaks at 1414 cm^{-1} and 874 cm^{-1} originate from the vibration of ν_3 [CO_3^{2-}] and ν_2 [CO_3^{2-}] respectively, which is coherent with the formation of calcite, hydrotalcite and hemicarbonate during the reaction. The sharp peaks at around 973 cm^{-1}, 817 cm^{-1} and 664 cm^{-1} in the spectrum represent the Si-O asymmetric stretching vibration and Si-O-Si bending vibration in the C-(A)-S-H gel [13,25]. Besides, both the increased Na_2CO_3 and WIFD content results in a sharper peak at around 817 cm^{-1}, indicating the formation of C-(A)-S-H gel [13]. The band centered around 1130 cm^{-1}, which is assigned to the ν_3 [SO_4^{2-}], is getting more intense in Fig. 12 (a) due to the increased WIFD content providing more sulfate ions. The gradually disappearing band centered at around 892 cm^{-1} is due to the presence of TO_4 (T is Si or Al) from the original slag [6;53], which was decreased after more slag was reacted. The results of 90% GGBFS and 10% WIFD blended samples activated by different amounts of Na_2CO_3 are shown in Fig. 12 (b) and exhibits similar resonances. Notably, Si-O stretching in C-(A)-S-H gel is shifted from 960 cm^{-1} to 936 cm^{-1}, indicating the decreased polymerization of C-(A)-S-H gel due to the lower proportion of GGBFS in the mixture.

3.3.3. TG-DTG analysis

Fig. 13 shows the TG-DTG results of Na_2CO_3 activated GGBFS samples with different WIFD replacements after 3 days. The first peak of DTG curves between 20 °C and 240 °C is associated with the dehydration of C-(A)-S-H gel, hemicarbonate and hydrotalcite. Notably, a distinct peak around 120 °C in Fig. 14 (a) is assigned to the dehydration of gaylussite [53], which is coherent with the observation with XRD results (Fig. 8, where the N8W0 is the only sample containing gaylussite. The small shoulders at around 200 °C are caused by the loss of the bound water from hydration products like hydrotalcite and hemicarbonate [21]. The portlandite from WIFD, visible in the XRD results, is supposed to decompose at around 430 °C. However, it's pretty difficult to identify the mass loss of portlandite due to the decarbonation of hydrotalcite that also occurs at 400 ~ 650 °C [9]. Besides, the portlandite would be consumed over time by the reaction with Na_2CO_3. The weight loss of around 700 °C is induced by the decarbonation of calcite originated from the raw material WIFD, as seen in the TG results in Fig. 2. The weight loss of around 800 °C is related to the decarbonation of carbonates which is newly formed or from the thermal decomposition of hydrotalcite or hemicarbonate during the TG test [43].

Table 5 summarizes the mass loss of the different phases at different temperature ranges. To evaluate the amount the formation of C-(A)-S-H gel, the mass loss between 40 °C and 150 °C are treated as bound water from the gel. Here the bound water from gaylussite which is only found in N8W0 is also included. Therefore, the calculated bound water in N8W0 would be higher than the theoretical value. As can be seen, the increased amount of bound water from 3 days to 91 days confirms the reaction process and the formation of hydration products. Theoretically, incorporating WIFD would decrease the bound water due to the reduced proportion of GGBFS in the mixture. However, the amount of bound water in N8W5-N8W20 is almost similar, indicating a higher reaction degree of GGBFS with more WIFD. Besides, the formation of hydrotalcite (400 ~ 650 °C) and hemicarbonate (as newly formed in Table 5

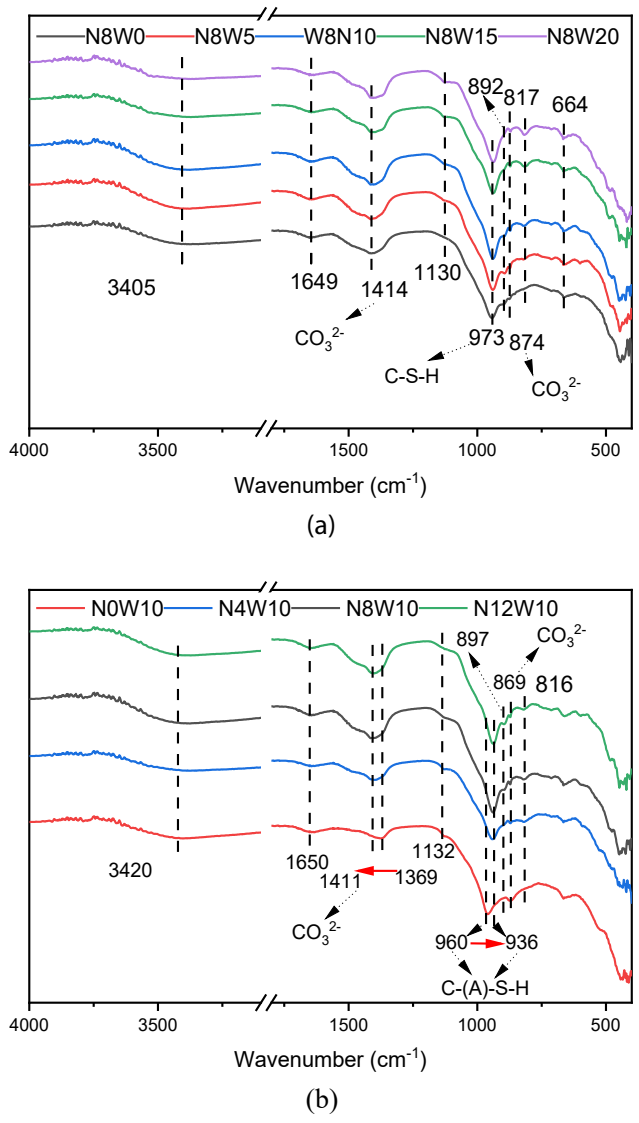

Fig. 12. FT-IR spectrum of mixtures after 28 days. (a) with different amounts of WIFD (b) with different amounts of Na_2CO_3.

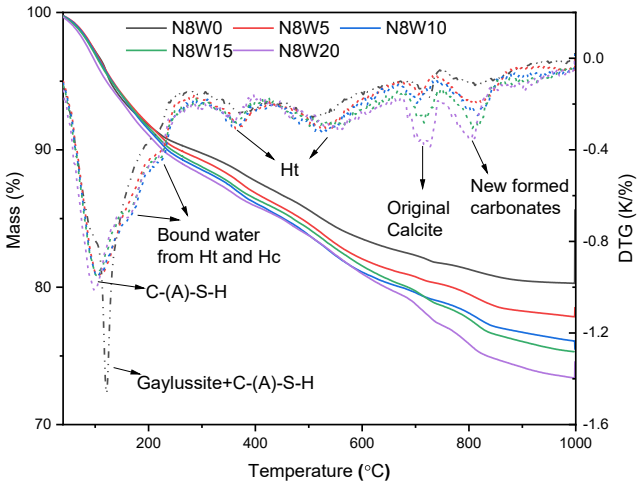

Fig. 13. TG-DTG curves of reaction products with different WIFD replacement after 3 days (Ht-Hydrotalcite, Hc-Hemicarbonate).

increases when more WIFD is incorporated. Then the mass loss between 650 °C and 760 °C is caused by the decarbonation of calcite from the WIFD, which is marked as "original calcite" in the WIFD (Fig. 2. Using the TG data from pure WIFD, it is possible to calculate the theoretical quantity of calcite from WIFD for each mixture. The amount of original calcite after hydration is lower than the theoretical amount due to the formation of hemicarbonate and hydrotalcite. To conclude, though the incorporation of WIFD decreases the proportion of GGBFS, it promotes the reaction degree of GGBFS and the formation of hydrotalcite and hemicabonate.

Fig. 15 shows the TG-DTG results of mixtures with different amounts of Na_2CO_3 at the curing ages of 3 days. The dehydration of the ettringite in mixture N0W10 is not visible because it overlaps with the dehydration of the C-(A)-S-H gel. The shoulder around 155 °C is due to the dehydration of hydrotalcite. The mass loss around 450 °C is only visible in N0W10 and is attributed to the portlandite from WIFD, which confirms the low reaction speed of mixture N0W10 at 3 days. The other mass loss is the decarbonation of carbonates as mentioned above.

Table 6 summarizes the mass loss of different phases at different temperature ranges. As can be seen, the bound water at 3d in N0W10 and N4W10 is relatively lower than that in N8W10 and N12W10, which is coherent with low reactivity at an early age in the calorimetric test. However, it shows a higher amount of bound water at 91 d in N0W10 than that in N4W10 due to the formation of ettringite. And with more Na_2CO_3 incorporated, the formation of hydrotalcite and hemicarbonate is increased, while the amount of calcite from the WIFD decreases in the samples. In general, Na_2CO_3 also plays a significant role in activating 90 % GGBFS and 10 % WIFD blends, which improve the alkali concentration by the reaction with portlandite in WIFD. Besides, Na_2CO_3 promotes the consumption of calcite from WIFD to form the hemicarbonate and hydrotalcite [53].

3.4. Gel microstructure

The morphology of the mixtures with different replacement levels of WIFD at 28 days and element compositions of reaction products are studied using SEM & EDX (Fig. 16. Notably, unreacted slag particles still exist in the inner matrix as seen in polished samples (Fig. 16. The flaky structures could be hydrotalcite [58]. Further details about the reaction products were determined through EDX spot measurements to determine the element composition on the polished surface. The results are summarised in Fig. 17. According to a study on a model for the C-A-S-H gel, the Ca/Si ratio is between 0.86 and 1.21 and the Al/Si ratio is between 0.22 and 0.42 in alkali-activated GGBFS [33]. The initial Ca/Si and Al/Si ratio in GGBFS, according to the chemical composition in Table 1 was calculated to be around 0.96 and 0.36, which is similar to those ratios in the C-A-S-H gel. However, there is no Na content in GGBFS, which is helpful to distinguish it from the reaction products, as seen in Fig. 17. Besides, the formation of hydrotalcite and calcite or dolomite according to the XRD results may lead to higher Al/Si and Ca/Si ratios, respectively, as indicated by the direction of arrows for the red spots in Fig. 17. And the formation of ettringite in N0W10 also leads to a higher Al/Si and Ca/Si ratio. Some spots around the unreacted GGBFS still contain sodium which indicates the potential formation of N-A-S-H gel.

The morphology of the 90% GGBFS and 10% WIFD blended mixtures activated by Na_2CO_3 at 28 days are investigated by using SEM (Fig. 18. As can be seen, the needle-like structures nearly cover the surface of the matrix in sample N0W10, indicating the formation of ettringite as found in XRD patterns in Fig. 11. Besides, the higher Ca/Al ratio in ettringite leads to a higher Al/Si ratio and Ca/Si ratio, as seen in Fig. 17. The silhouette of unreacted slag grain can still be found in both N0W10 and N4W10. The porous structure on the surface in N4W10 indicates the number of reaction products is not enough to fill the pores due to the low reaction degree of GGBFS. The small calcite grains and the flaky hydrotalcite are found in each mixture. The formed particle size of flaky

Table 5
Weight loss (wt%) of each phase with the temperature range.

	Dehydration of Bound water 40 ~ 150 °C			Decarbonation of Hydrotalcite 400 ~ 650 °C			Decarbonation of Carbonates 650 ~ 760 °C			Calcite fromWIFD	Newly formed carbonates 760 ~ 850 °C		
	3d	28d	91d	3d	28d	91d	3d	28d	91d		3d	28d	91d
N8W0	6.1	8.4	17.4	0.6	0.6	0.4	0.3	0.2	0.1	0	0.5	0.1	0.1
N8W5	5.7	8.4	16.8	1.2	1.4	1.1	0.2	0.2	0.2	0.5	1.0	1.1	0.2
N8W10	5.8	7.9	15.1	1.3	1.6	1.3	0.3	0.3	0.3	1.0	0.9	1.4	0.7
N8W15	5.7	7.7	16.4	1.7	1.5	1.1	0.5	0.6	0.3	1.6	1.2	1.3	1.2
N8W20	6.2	7.1	15.2	1.5	1.4	0.9	0.9	1.1	0.4	2.1	1.1	1.0	1.4

Table 6
Weight loss of each phase with the temperature range (by percentage).

	Dehydration of Bound water 40 ~ 150 °C			Decarbonation of Hydrotalcite 400 ~ 650 °C			Decarbonation of Carbonates 650 ~ 760 °C			Calcite from WIFD	Newly formed carbonates 760 ~ 850 °C		
	3d	28d	91d	3d	28d	91d	3d	28d	91d		3d	28d	91d
N0W10	3.6	5.3	17.2	0.7	0.9	0.1	0.7	0.4	0.2	1.1	0.2	0.5	0.6
N4W10	4.1	5.0	6.0	1.4	1.2	1.1	0.5	0.6	0.3	1.1	0.7	0.2	0.9
N8W10	5.8	7.9	15.0	1.3	1.6	1.3	0.3	0.3	0.3	1.0	0.9	1.4	0.7
N12W10	6.0	8.0	16.9	1.4	1.9	0.7	0.2	0.2	0.2	1.0	1.0	1.5	1.8

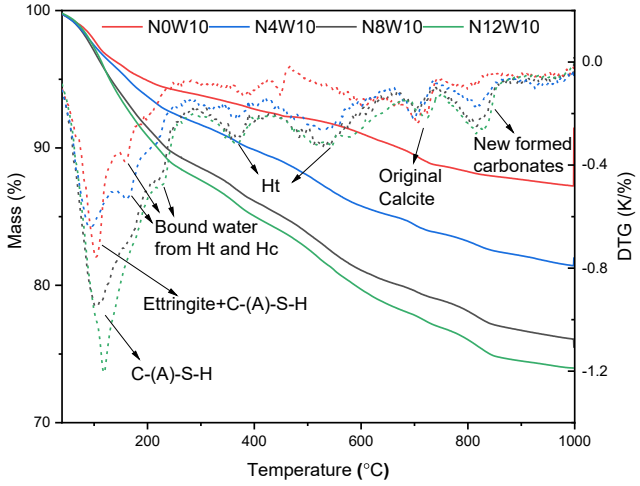

Fig. 14. TG-DTG curves of reaction products with different amounts of additional Na_2CO_3 after 3 days (Ht-Hydrotalcite, Hc-Hemicarbonate).

hydrotalcite grows up gradually with increased Na_2CO_3 from N4W10 to N12W10.

Fig. 19 (a) shows the cumulative pore volume of paste samples with different proportions of WIFD after 28 days of curing. It can be seen that the incorporation of WIFD significantly influences the total pore volume of the Na_2CO_3 activated GGBFS. At low replacement levels of from 5% to 10%, the total gel porosity of the samples is decreased due to the filling effect of hemicarbonate and hydrotalcite formed in the reaction. However, samples of high replacement ratios around 15 ~ 20% show the opposite trends. This could be explained by two reasons. At first, the reduced amount of GGBFS in the binder leads to a reduction of hydration products (e.g. CASH) which forms in the pore structure. Secondly, as the water to binder (GGBFS and WIFD) ratio is kept the same, higher amounts of WIFD in the reaction system lead to a reduction in flowability as in Fig 0.4 because of the high water demand of WIFD. Then, the low flowability results in high gel porosity.

The pore size distribution of the paste between 2 and 200 nm is presented in Fig. 19 (b). Generally, the gel pores (less than 10 nm) and capillary pores (10 ~ 100 nm) are the two main classes of pores [31]. As can be seen, the reference group shows a smaller critical size of the pores indicating a less porous structure filling with more reaction products. Then with the increased WIFD in the mixtures, the porosity of gel pores was increased due to the promoted reaction process by the WIFD. However, it also increases the volume of capillary pores, which was induced by the degradation of flowability due to the incorporation of WIFD. Besides, the formation of hydrotalcite and hemicarbonate is increased even though only 5% WIFD was applied as shown in Table 5, which is significant for the reducing gel porosity. However, a further increase of the WIFD content shows no effect on the critical pore size.

Fig. 20 (a) shows the cumulative pore volume of 90% GGBFS and 10% WIFD blended paste with different amounts of Na_2CO_3 after 28 days of curing. The cumulative pore volume of the slag pastes decreases from 0.1276 cm^3/g to 0.0236 cm^3/g with the increase of Na_2CO_3 content. Obviously, the pore structure is filled with the reaction products such as the hydrotalcite, hemicarbonate and C/N-(A)-S-H gel to form a more compact structure according to SEM results (Fig. 19. The pore size distribution of the paste between 2 and 200 nm is presented in Fig. 20 (b). The increase of the Na_2CO_3 content would improve the porous structure of the matrix and the critical pore size decreases from 90 nm to 40 nm. However, the dosage of Na_2CO_3 makes the differences in the formation quantity of products which would be helpful to reduce the porosity of the matrix and form a denser structure.

3.5. Mechanical properties

The compressive strength of Na_2CO_3 activated mixture with different amounts of WIFD after 7 days, 28 days and 91 days curing are shown in Fig. 21. Understandably, the more slag replaced by WIFD leads to a reduction of the compressive strength. The formation of C/N-(A)-S-H gel as the main contribution to the mechanical properties of samples, is limited by the GGBFS content rather than WIFD. As shown in Table 5, though the bound water/ GGBFS of each mixture is comparable, the total bound water content decreases with the reduced GGBFS. The reduced compressive strength is also coherent with cumulative pore volume in Fig. 20 (a) because WIFD increases higher pore volume. The reduction of flowability caused by the WIFD addition may also lead to higher pore defects. However, the mechanical performance of samples is still high enough for a potential application in construction with lower strength requirements.

The compressive strength of 90% GGBFS and 10% WIFD blend binder with various Na_2CO_3 at the curing ages of 7 days, 28 days and 91 days are shown in Fig. 22. The mixture without Na_2CO_3 (N0W8) still presents a compressive strength. Besides, the N0W10 shows better mechanical property than that of the N4W10, which is possible to be induced by the formation of ettringite in N0W10, reducing the porosity

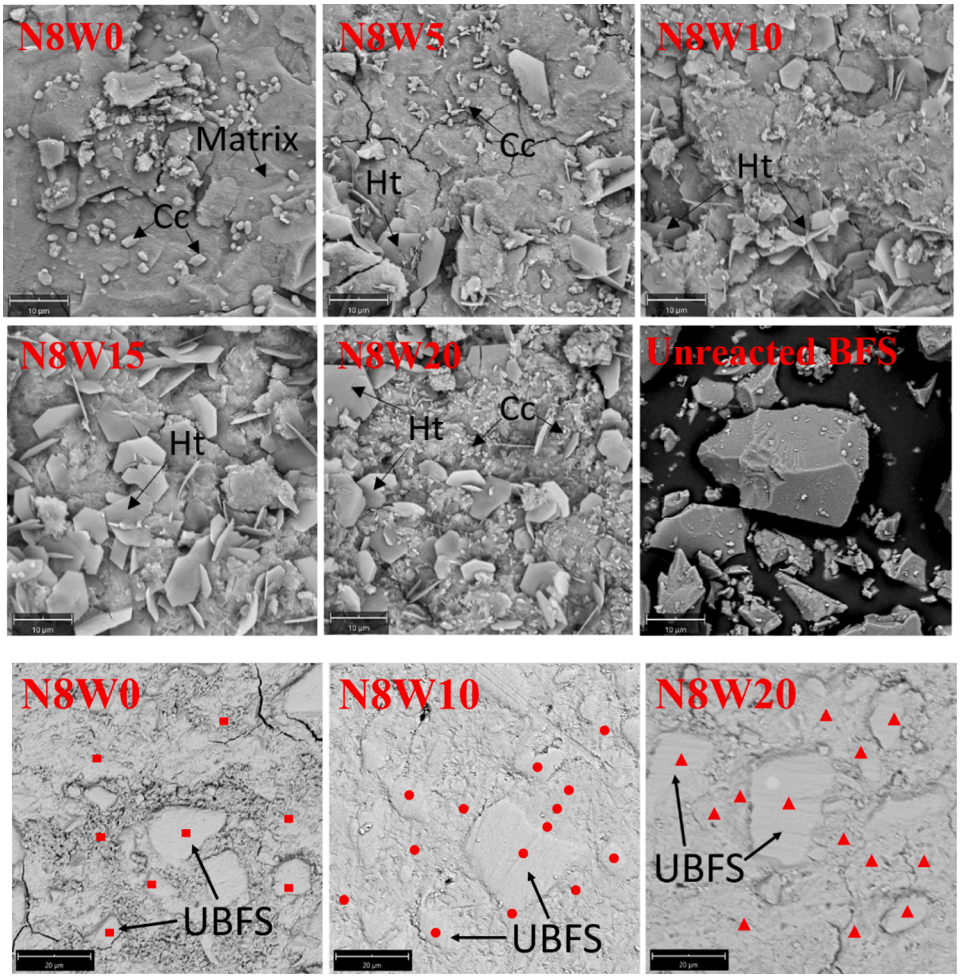

Fig. 16. SEM (polished samples used in Fig. 18 images of mixtures at 28d. (Ht-Hydrotalcite, Cc-Calcite, UBFS-Unreacted GGBFS) The red points mark the measurement spots in Fig. 17.

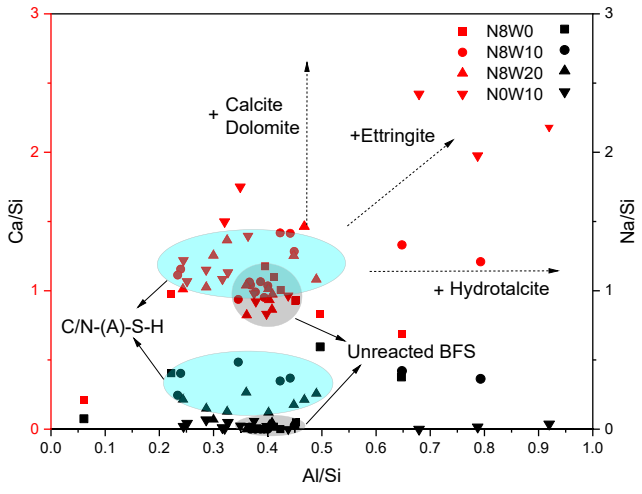

Fig. 17. Plot of EDX spot map atomic ratios comparing Ca/Si and Na/Si to Al/Si in the matrix. (black spots for the Ca/Si and red spots for the Na/Si).

of the samples. When the additional amount of Na_2CO_3 is up to 8% by mass, the compressive strength is increased significantly due to the higher reaction degree of GGBFS. When the additional amount of Na_2CO_3 is 12% by mass, the compressive strength shows no further increase due to the limited proportion of GGBFS in the mixture.

3.6. Role of WIFD and Na_2CO_3

Previously, Akturk and Kizilkanat [2] investigated the effect of Ca $(OH)_2$ on Na_2CO_3 activated blast furnace slag and reported that the use of lime would decrease the concentration of CO_3^{2-} in the pore solution. Meanwhile, the fresh state behavior of Na_2CO_3 activated slag paste was well investigated, determining setting time, pH of pore solution and rheological properties [2]. Some similar results are achieved in this work when the WIFD is used as a green $Ca(OH)_2$ source in the Na_2CO_3 activated GGBFS. However, the performance of Na_2CO_3 activated slag with WIFD at the longer curing ages was studied in this work, including the reaction assemblage, the mechanical properties and gel microstructure. As shown in Fig. 23, WIFD is composed of portlandite and calcite, portlandite provides the OH^- through the reaction with sodium carbonate; part of calcite would be consumed to form the hydrotalcite and hemicarbonate. Further details about the effects of WIFD on the sodium carbonate activated GGBFS were divided into chemical and physical aspects.

3.6.1. Chemical effect

The addition of WIFD effectively affects the reaction process of Na_2CO_3 activated GGBFS systems. Even 5% WIFD in the reaction system could reduce the time to reach the heat flow peak from 2 days to 9 h. At first, the Ca concentration (from portlandite and calcite) can be increased during an initial period, and the increased Ca/Si ratio would influence the structure of the formed gels. Secondly, portlandite in WIFD provides a higher initial pH than Na_2CO_3, as the initial pH value is a

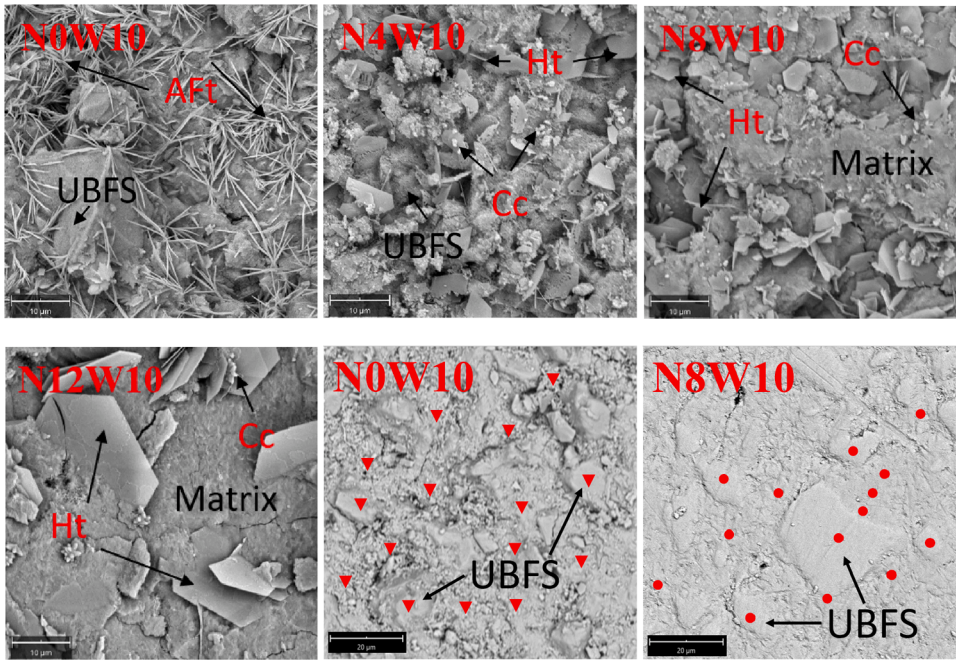

Fig. 18. SEM and BSE (polished samples used in Fig. 18 images of mixtures at 28d (Aft-Ettringite, Ht-Hydrotalcite, Cc-Calcite, UBFS-Unreacted GGBFS). The red points mark the measurement spots shown in Fig. 17.

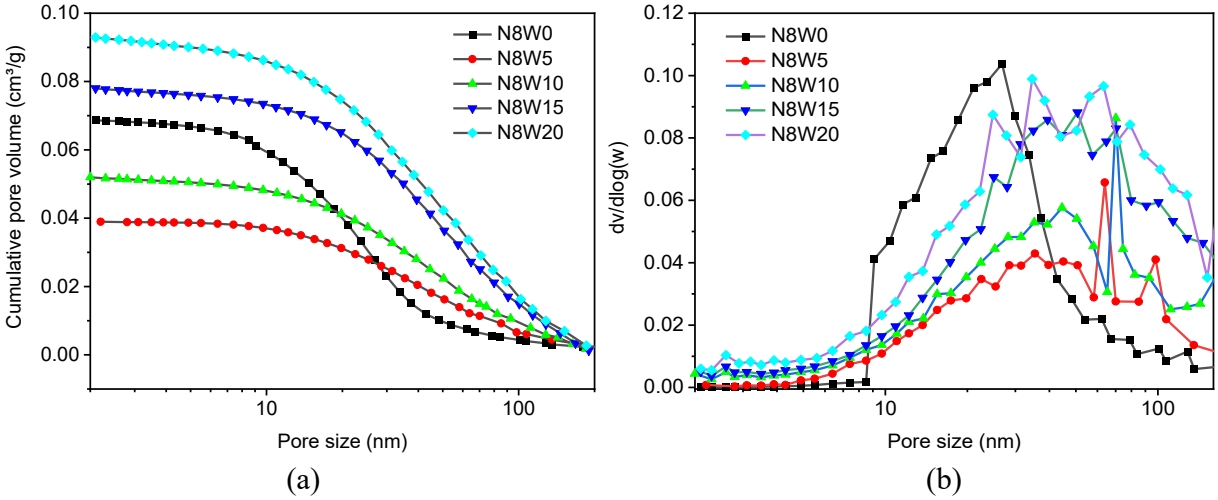

Fig. 19. Samples with different replacement of WIFD from BJH adsorption: a - Cumulative pore volume, b - Pore size distribution.

significant factor in the hydration rate [8,40]. The reaction between portlandite and Na_2CO_3 promotes the further increase of pH [4,22]. Finally, the formation of hemicarbonate benefits from the calcite originated from WIFD.

Besides, it's proved that the GGBFS could be activated by the WIFD alone (N0W10), with the main reaction products such as ettringite, hydrotalcite and C/N-(A)-S-H gel, which corresponds to the previous results reported by Mobasher and Bernal [32]. However, the formation of hemicarbonate was identified in this work due to the initial calcite from the WIFD, which did not exist in a previous study on the hydrated-lime activated GGBFS [19]. In addition, the effect of limestone powder in Na_2CO_3 activated GGBFS was revealed by Yuan et al. [54], and the formation of hemicarbonate was not observed either in the Na_2CO_3 activated GGBFS system without portlandite. Therefore, the portlandite and calcite from WIFD show a significant role in the formation of hemicarbonate. When Na_2CO_3 and WIFD were used together as in sample N8W10, the ettringite did not form, indicating that Al^{3+} was consumed for the formation of hydrotalcite ($Mg_6Al_2CO_3(OH)_{16}{\cdot}4H_2O$) promoted by the Na_2CO_3. In general, WIFD and Na_2CO_3 have synergy in the reaction process by the improving pH value and both can affect the types of reaction products.

3.6.2. *Physical effect*

As we found in the flowability test of mortar samples, the incorporation of WIFD results in a reduction of flowability, which probably causes high porosity and reduces compressive strength. However, low WIFD (N8W5 and N8W10) could decrease the cumulate pore volume, indicating that the reaction products promoted by WIFD show a filling effect in the pore. Therefore, the low replacement of WIFD (5% ~10%) with additional proper superplasticizers would be beneficial to improve the fresh workability and gel porosity of the matrix.

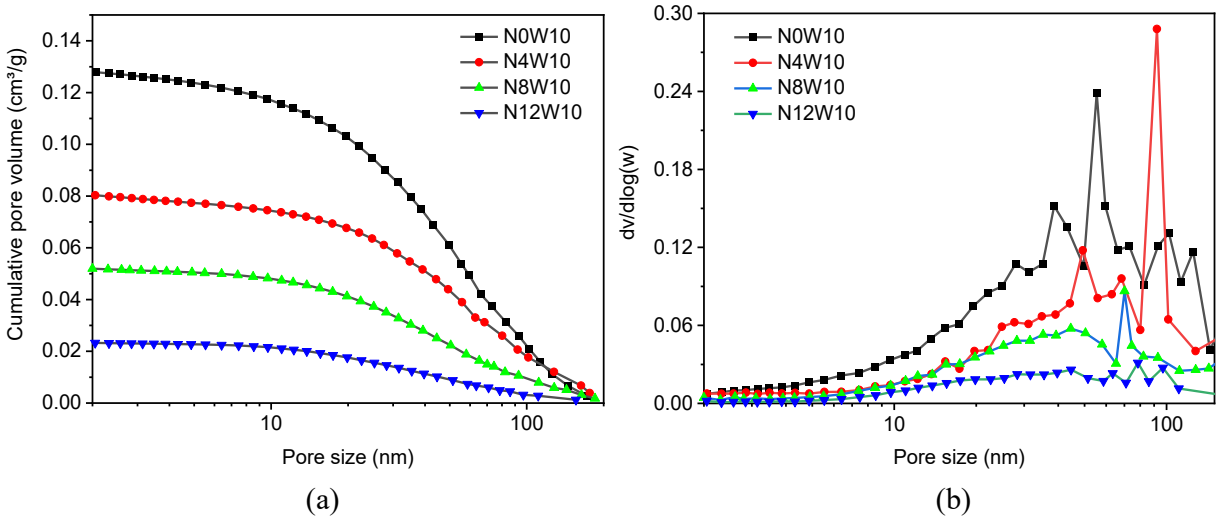

Fig. 20. Samples with different amounts of Na_2CO_3 from BJH adsorption. a - Cumulative pore volume, b - Pore size distribution.

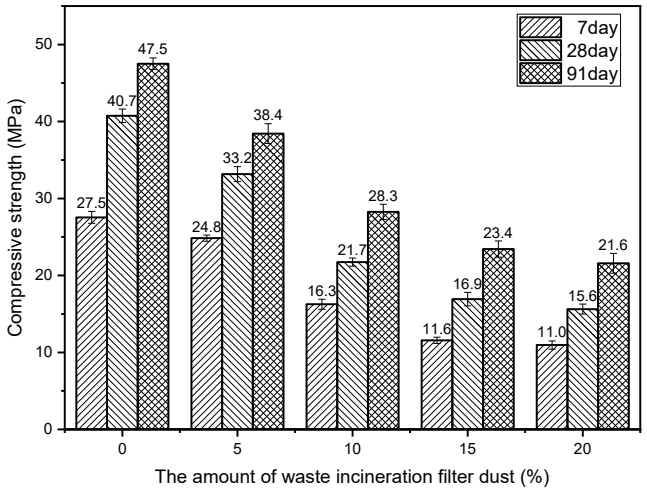

Fig. 21. Effect of WIFD content and curing age on the compressive strength of materials.

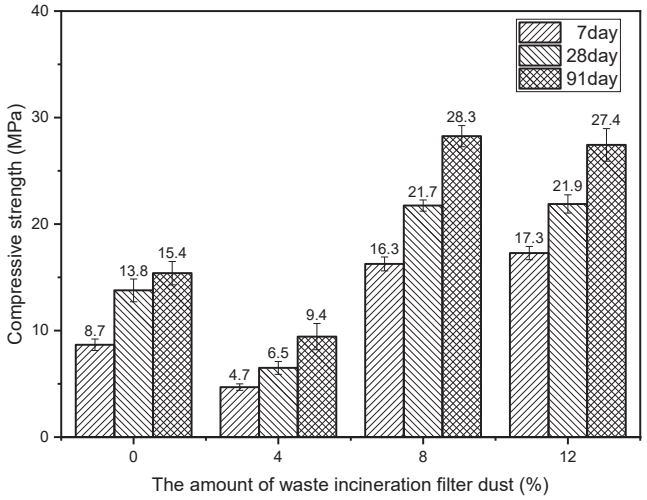

Fig. 22. Effect of Na_2CO_3 and curing age on the compressive strength of mortars.

4. Conclusions

This work aims to utilize waste incineration filter dust (WIFD) in sodium carbonate activated slag. The workability, reaction kinetics, reaction products of GGBFS activated by WIFD and Na_2CO_3 are characterized by isothermal calorimetry, XRD, TG-DTG, FT-IR and SEM. Furthermore, the influence of WIFD content, Na_2CO_3 dosages and curing ages on the workability and mechanical properties was investigated. The following conclusions can be drawn according to the obtained results.

1. The incorporation of WIFD would reduce the workability of the mortar due to its high-water demand. The mixture with low WIFD content shows proper workability. It is recommended to use superplasticizers to adjust its workability in the high replacement of WIFD.
2. When Na_2CO_3 or WIFD activates GGBFS along, it shows a prolonged reaction process with nearly 2 d to reach the heat flow peak. Na_2CO_3 and WIFD have a synergistic effect on the activation of GGBFS. The initial alkalinity of the pore solution is raised by the reaction between Na_2CO_3 and WIFD, which leads to the acceleration of the reaction process. For example, the time to reach the heat flow peak is reduced from 58 h to 10 h by 5% WIFD.
3. The main reaction products in the NC-WIFD-GGBFS blends are hemicarbonate, hydrotalcite and C-(A)-S-H gels. WIFD and Na_2CO_3 significantly promote the formation of hemicarbonate and hydrotalcite. The formation of ettringite is only observed in the WIFD-GGBFS blends, indicating that additional Na_2CO_3 consumes aluminum ions to form the hydrotalcite preferentially.
4. In the NC-WIFD-GGBFS blends, the replacement level of WIFD and the dosage of Na_2CO_3 are crucial for the microstructure of the matrix. Though the incorporation of WIFD improves the gels content and gel porosity, it also leads to a reduction of workability and induces more capillary pores. On the contrary, Na_2CO_3 is beneficial to form a denser structure with lower gel porosity.
5. WIFD and Na_2CO_3 show the different effects on the mechanical properties of the NC-WIFD-GGBFS blends. More WIFD reduces the compressive strength due to the lowered proportion of GGBFS. Na_2CO_3 improves the compressive strength of the mortar by the accelerated reaction process and products.
6. The work shows an alternative approach to green building materials prepared with blast furnace slag and Waste incineration filter dust (WIFD). The use of WIFD in the system can help save energy, reduce CO_2 emissions and provide an application for WIFD. Further studies will focus on improving the utilization of waste incineration filter

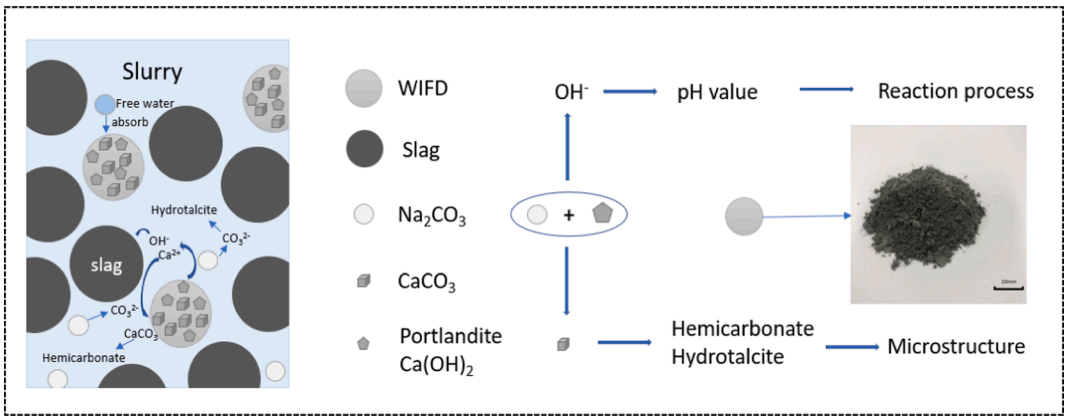

Fig. 23. Schematics of the reaction mechanism in the NC-WIFD-GGBFS blends.

dust (WIFD) in the AAMs with higher mechanical properties. The durability of NC-WIFD-GGBFS blends will be investigated.

Declaration of Competing Interest

The authors declare that they have no known competing financial interests or personal relationships that could have appeared to influence the work reported in this paper.

Acknowledgment

This research was supported by the funding of the China Scholarship Council (No. 201906950015) and Eindhoven University of Technology. The authors would like to thank Euro Trust Management for the supply of waste incineration filter dust.

Appendix A. Supplementary data

Supplementary data to this article can be found online at https://doi.org/10.1016/j.conbuildmat.2021.125494.

References

[1] A. Abdalqader, F. Jin, A. Al-Tabbaa, Performance of magnesia-modified sodium carbonate-activated slag/fly ash concrete, Cem. Concr. Compos. 103 (2019) 160–174, https://doi.org/10.1016/j.cemconcomp.2019.05.007.
[2] B. Akturk, A.B. Kizilkanat, N. Kabay, Effect of calcium hydroxide on fresh state behavior of sodium carbonate activated blast furnace slag pastes, Constr. Build. Mater. 212 (2019) 388–399, https://doi.org/10.1016/j.conbuildmat.2019.03.328.
[3] E. Altan, S.T. Erdoğan, Alkali activation of a slag at ambient and elevated temperatures, Cem. Concr. Compos. 34 (2) (2012) 131–139, https://doi.org/10.1016/j.cemconcomp.2011.08.003.
[4] S.A. Bernal, J.L. Provis, R.J. Myers, R. San Nicolas, J.S.J. van Deventer, Role of carbonates in the chemical evolution of sodium carbonate-activated slag binders, Mater. Struct. Constr. 48 (3) (2015) 517–529, https://doi.org/10.1617/s11527-014-0412-6.
[5] S.A. Bernal, J.L. Provis, V. Rose, R. Mejía de Gutierrez, Evolution of binder structure in sodium silicate-activated slag-metakaolin blends, Cem. Concr. Compos. 33 (1) (2011) 46–54, https://doi.org/10.1016/j.cemconcomp.2010.09.004.
[6] S.A. Bernal, E.D. Rodríguez, R. Mejia de Gutiérrez, J.L. Provis, S. Delvasto, Activation of metakaolin/slag blends using alkaline solutions based on chemically modified silica fume and rice husk ash, Waste Biomass Valorizat. 3 (1) (2012) 99–108, https://doi.org/10.1007/s12649-011-9093-3.
[7] S. Brunauer, P.H. Emmett, E. Teller, Adsorption of Gases in Multimolecular Layers, J. Am. Chem. Soc. 60 (2) (1938) 309–319.
[8] C. Shi, R.L.D., 1995. Day A calorimetric study of early hydration of alkali.pdf. Cem. Concr. Res. 25, 1333–1346.
[9] N.T. Dung, T.J.N. Hooper, C. Unluer, Accelerating the reaction kinetics and improving the performance of Na2CO3-activated GGBS mixes, Cem. Concr. Res. 126 (2019) 105927, https://doi.org/10.1016/j.cemconres.2019.105927.
[10] C. Duran Atiş, C. Bilim, Özlem Çelik, O. Karahan, Influence of activator on the strength and drying shrinkage of alkali-activated slag mortar, Constr. Build. Mater. 23 (1) (2009) 548–555, https://doi.org/10.1016/j.conbuildmat.2007.10.011.
[11] A. Fernandez-Jimenez, F. Puertas, Setting of alkali-activated slag cement. Influence of activator nature, Adv. Cem. Res. 13 (3) (2001) 115–121, https://doi.org/10.1680/adcr.2001.13.issue-310.1680/adcr.13.3.115.39288.
[12] I. Garcia-Lodeiro, A. Palomo, A. Fernández-Jiménez, D.E. Macphee, Compatibility studies between N-A-S-H and C-A-S-H gels. Study in the ternary diagram Na2O-CaO-Al2O3-SiO 2–H2O, Cem. Concr. Res. 41 (9) (2011) 923–931, https://doi.org/10.1016/j.cemconres.2011.05.006.
[13] I. García Lodeiro, D.E. Macphee, A. Palomo, A. Fernández-Jiménez, Effect of alkalis on fresh C-S-H gels, FTIR analysis. Cem. Concr. Res. 39 (3) (2009) 147–153, https://doi.org/10.1016/j.cemconres.2009.01.003.
[14] M.B. Haha, B. Lothenbach, G. Le Saout, F. Winnefeld, Influence of slag chemistry on the hydration of alkali-activated blast-furnace slag - Part II: Effect of Al2O3, Cem. Concr. Res. 42 (1) (2012) 74–83, https://doi.org/10.1016/j.cemconres.2011.08.005.
[15] X. He, Z. Zheng, J. Yang, Y. Su, T. Wang, B. Strnadel, Feasibility of incorporating autoclaved aerated concrete waste for cement replacement in sustainable building materials, J. Clean. Prod. 250 (2020) 119455, https://doi.org/10.1016/j.jclepro.2019.119455.
[16] S. Houngaloune, K.S. Ariffin, H.B. Hussin, K. Watanabe, V. Nhinxay, The effects of limestone characteristic, granulation and calcination temperature to the reactivity of quicklime, Malaysian J. Microsc. 6 (2010) 53–57.
[17] I. Ismail, S.A. Bernal, J.L. Provis, R. San Nicolas, S. Hamdan, J.S.J. Van Deventer, Modification of phase evolution in alkali-activated blast furnace slag by the incorporation of fly ash, Cem. Concr. Compos. 45 (2014) 125–135, https://doi.org/10.1016/j.cemconcomp.2013.09.006.
[18] D. Jeon, Y. Jun, Y. Jeong, J.E. Oh, Microstructural and strength improvements through the use of Na2CO3 in a cementless Ca(OH)2-activated Class F fly ash system, Cem. Concr. Res. 67 (2015) 215–225, https://doi.org/10.1016/j.cemconres.2014.10.001.
[19] Y. Jeong, J.E. Oh, Y. Jun, J. Park, J.H. Ha, S.G. Sohn, Influence of four additional activators on hydrated-lime [Ca(OH)2] activated ground granulated blast-furnace slag, Cem. Concr. Compos. 65 (2016) 1–10, https://doi.org/10.1016/j.cemconcomp.2015.10.007.
[20] M.C.G. Juenger, R. Siddique, Recent advances in understanding the role of supplementary cementitious materials in concrete, Cem. Concr. Res. 78 (2015) 71–80, https://doi.org/10.1016/J.CEMCONRES.2015.03.018.
[21] X. Ke, S.A. Bernal, J.L. Provis, Uptake of chloride and carbonate by Mg-Al and Ca-Al layered double hydroxides in simulated pore solutions of alkali-activated slag cement, Cem. Concr. Res. 100 (2017) 1–13, https://doi.org/10.1016/j.cemconres.2017.05.015.
[22] X. Ke, S.A. Bernal, J.L. Provis, Controlling the reaction kinetics of sodium carbonate-activated slag cements using calcined layered double hydroxides, Cem. Concr. Res. 81 (2016) 24–37, https://doi.org/10.1016/j.cemconres.2015.11.012.
[23] M. Khachani, A. El Hamidi, M. Halim, S. Arsalane, Non-isothermal kinetic and thermodynamic studies of the dehydroxylation process of synthetic calcium hydroxide Ca(OH) 2, J. Mater. Environ. Sci. 5 (2014) 615–624.
[24] M.S. Kim, Y. Jun, C. Lee, J.E. Oh, Use of CaO as an activator for producing a price-competitive non-cement structural binder using ground granulated blast furnace slag, Cem. Concr. Res. 54 (2013) 208–214, https://doi.org/10.1016/j.cemconres.2013.09.011.
[25] Y. Kocak, S. Nas, The effect of using fly ash on the strength and hydration characteristics of blended cements, Constr. Build. Mater. 73 (2014) 25–32, https://doi.org/10.1016/j.conbuildmat.2014.09.048.
[26] N.K. Lee, H.K. Lee, Setting and mechanical properties of alkali-activated fly ash/slag concrete manufactured at room temperature, Constr. Build. Mater. 47 (2013) 1201–1209, https://doi.org/10.1016/j.conbuildmat.2013.05.107.
[27] C. Li, H. Sun, L. Li, A review: The comparison between alkali-activated slag (Si + Ca) and metakaolin (Si + Al) cements, Cem. Concr. Res. 40 (9) (2010) 1341–1349, https://doi.org/10.1016/j.cemconres.2010.03.020.
[28] N. Li, C. Shi, Z. Zhang, Understanding the roles of activators towards setting and hardening control of alkali-activated slag cement, Compos. Part B Eng. 171 (2019) 34–45, https://doi.org/10.1016/j.compositesb.2019.04.024.
[29] G. Liu, M.V.A. Florea, H.J.H. Brouwers, Performance evaluation of sustainable high strength mortars incorporating high volume waste glass as binder, Constr. Build. Mater. 202 (2019) 574–588, https://doi.org/10.1016/J.CONBUILDMAT.2018.12.110.

[30] G. Liu, K. Schollbach, P. Li, H.J.H. Brouwers, Valorization of converter steel slag into eco-friendly ultra-high performance concrete by ambient CO2 pre-treatment, Constr. Build. Mater. 280 (2021) 122580, https://doi.org/10.1016/j.conbuildmat.2021.122580.
[31] Y. Ma, J. Hu, G. Ye, The pore structure and permeability of alkali activated fly ash, Fuel 104 (2013) 771–780, https://doi.org/10.1016/j.fuel.2012.05.034.
[32] N. Mobasher, S.A. Bernal, J.L. Provis, Structural evolution of an alkali sulfate activated slag cement, J. Nucl. Mater. 468 (2016) 97–104, https://doi.org/10.1016/j.jnucmat.2015.11.016.
[33] F. Puertas, M. Palacios, H. Manzano, J.S. Dolado, A. Rico, J. Rodríguez, A model for the C-A-S-H gel formed in alkali-activated slag cements, J. Eur. Ceram. Soc. 31 (12) (2011) 2043–2056, https://doi.org/10.1016/j.jeurceramsoc.2011.04.036.
[34] M.J. Quina, João.C. Bordado, R.M. Quinta-Ferreira, Treatment and use of air pollution control residues from MSW incineration: An overview, Waste Manag. 28 (11) (2008) 2097–2121, https://doi.org/10.1016/j.wasman.2007.08.030.
[35] Rodriguez-Navarro, C., Ruiz-Agudo, E., Luque, A., Rodriguez-Navarro, A.B., Ortega-Huertas, M., 2009. Thermal decomposition of calcite: Mechanisms of formation and textural evolution of CaO nanocrystals. Am. Mineral. 94, 578–593. 10.2138/am.2009.3021.
[36] T. Sabbas, A. Polettini, R. Pomi, T. Astrup, O. Hjelmar, P. Mostbauer, G. Cappai, G. Magel, S. Salhofer, C. Speiser, S. Heuss-Assbichler, R. Klein, P. Lechner, Management of municipal solid waste incineration residues, Waste Manag. 23 (1) (2003) 61–88, https://doi.org/10.1016/S0956-053X(02)00161-7.
[37] M. Schneider, M. Romer, M. Tschudin, H. Bolio, Sustainable cement production-present and future, Cem. Concr. Res. 41 (7) (2011) 642–650, https://doi.org/10.1016/j.cemconres.2011.03.019.
[38] Z. Shi, C. Shi, S. Wan, N. Li, Z. Zhang, Effect of alkali dosage and silicate modulus on carbonation of alkali-activated slag mortars, Cem. Concr. Res. 113 (2018) 55–64, https://doi.org/10.1016/j.cemconres.2018.07.005.
[39] R. Shirley, L. Black, Alkali activated solidification/stabilisation of air pollution control residues and co-fired pulverised fuel ash, J. Hazard. Mater. 194 (2011) 232–242, https://doi.org/10.1016/J.JHAZMAT.2011.07.100.
[40] S. Song, H.M. Jennings, Pore solution chemistry of alkali-activated ground granulated blast-furnace slag, Cem. Concr. Res. 29 (1999) 159–170, https://doi.org/10.1016/S0008-8846(98)00212-9.
[41] B. Walkley, R. San Nicolas, M.A. Sani, G.J. Rees, J.V. Hanna, J.S.J. van Deventer, J. L. Provis, Phase evolution of C-(N)-A-S-H/N-A-S-H gel blends investigated via alkali-activation of synthetic calcium aluminosilicate precursors, Cem. Concr. Res. 89 (2016) 120–135, https://doi.org/10.1016/j.cemconres.2016.08.010.
[42] Walling, S.A., Bernal, S.A., Gardner, L.J., Kinoshita, H., Provis, J., 2018. Blast furnace slag-Mg(OH)2 cements activated by sodium carbonate. RSC Adv. 8, 23101–23118. 10.1039/c8ra03717e.
[43] K. Wang, D. Han, P. Zhao, X. Hu, Z. Yin, D. Wu, Role of MgxCa1-xCO3 on the physical-chemical properties and cyclic CO2 capture performance of dolomite by two-step calcination, Thermochim. Acta 614 (2015) 199–206, https://doi.org/10.1016/j.tca.2015.06.033.
[44] J. Yang, H. Hu, X. He, Y. Su, Y. Wang, H. Tan, H. Pan, Effect of steam curing on compressive strength and microstructure of high volume ultrafine fly ash cement mortar, Constr. Build. Mater. 266 (2021) 120894, https://doi.org/10.1016/j.conbuildmat.2020.120894.
[45] J. Yang, J. Huang, Y. Su, X. He, H. Tan, W. Yang, B. Strnadel, Eco-friendly treatment of low-calcium coal fly ash for high pozzolanic reactivity. A step towards waste utilization in sustainable building material, J. Clean. Prod. 238 (2019) 117962, https://doi.org/10.1016/j.jclepro.2019.117962.
[46] J. Yang, J. Zeng, X. He, Y. Su, H. Tan, B. Strnadel, Nano-carbide slag seed as a new type accelerator for Portland cement, Mater. Lett. 278 (2020) 128464, https://doi.org/10.1016/j.matlet.2020.128464.
[47] J. Yang, L. Zeng, Z. Su, X. He, Y. Su, R. Zhao, X. Gan, Wet-milling disposal of autoclaved aerated concrete demolition waste – A comparison with classical supplementary cementitious materials, Adv. Powder Technol. 31 (9) (2020) 3736–3746, https://doi.org/10.1016/j.apt.2020.07.016.
[48] K.H. Yang, A.R. Cho, J.K. Song, S.H. Nam, Hydration products and strength development of calcium hydroxide-based alkali-activated slag mortars, Constr. Build. Mater. 29 (2012) 410–419, https://doi.org/10.1016/j.conbuildmat.2011.10.063.
[49] K.-H. Yang, J.-I. Sim, S.-H. Nam, Enhancement of reactivity of calcium hydroxide-activated slag mortars by the addition of barium hydroxide, Constr. Build. Mater. 24 (3) (2010) 241–251, https://doi.org/10.1016/j.conbuildmat.2009.09.001.
[50] T. Yang, Z. Zhang, H. Zhu, W. Zhang, Y. Gao, X. Zhang, Q. Wu, Effects of calcined dolomite addition on reaction kinetics of one-part sodium carbonate-activated slag cements, Constr. Build. Mater. 211 (2019) 329–336, https://doi.org/10.1016/j.conbuildmat.2019.03.245.
[51] N. Ye, Y. Chen, J. Yang, S. Liang, Y. Hu, J. Hu, S. Zhu, W. Fan, B. Xiao, Transformations of Na, Al, Si and Fe species in red mud during synthesis of one-part geopolymers, Cem. Concr. Res. 101 (2017) 123–130, https://doi.org/10.1016/j.cemconres.2017.08.027.
[52] B. Yuan, C. Straub, S. Segers, Q.L. Yu, H.J.H. Brouwers, Sodium carbonate activated slag as cement replacement in autoclaved aerated concrete, Ceram. Int. 43 (8) (2017) 6039–6047, https://doi.org/10.1016/j.ceramint.2017.01.144.
[53] B. Yuan, Q.L. Yu, H.J.H. Brouwers, Time-dependent characterization of Na2CO3 activated slag, Cem. Concr. Compos. 84 (2017) 188–197, https://doi.org/10.1016/j.cemconcomp.2017.09.005.
[54] B. Yuan, Q.L. Yu, H.J.H. Brouwers, Assessing the chemical involvement of limestone powder in sodium carbonate activated slag, Mater. Struct. Constr. 50 (2017), https://doi.org/10.1617/s11527-017-1003-0.
[55] B. Yuan, Q.L. Yu, H.J.H. Brouwers, Evaluation of slag characteristics on the reaction kinetics and mechanical properties of Na2CO3 activated slag, Constr. Build. Mater. 131 (2017) 334–346, https://doi.org/10.1016/j.conbuildmat.2016.11.074.
[56] B. Yuan, S. Yuan, C. Straub, W. Chen, Activation of Binary Binder Containing Fly Ash and Portland Cement Using Red Mud as Alkali Source and Its Application in Controlled Low-Strength Materials, J. Mater. Civ. Eng. 32 (2020) 1–11, https://doi.org/10.1061/(ASCE)MT.1943-5533.0003023.
[57] X.H. Yuan, W. Chen, Z.A. Lu, H. Chen, Shrinkage compensation of alkali-activated slag concrete and microstructural analysis, Constr. Build. Mater. 66 (2014) 422–428, https://doi.org/10.1016/j.conbuildmat.2014.05.085.
[58] H.Y. Zeng, X. Deng, Y.J. Wang, K.B. Liao, Preparation of mg-ai hydrotalcite by urea method and its catalytic activity for transesterification, AIChE J. 55 (2009) 1229–1235, https://doi.org/10.1002/AIC.11722.